

Optical crossover phenomenon due to a central 90°-twist defect in a chiral sculptured thin film or chiral liquid crystal

BY FEI WANG AND AKHLESH LAKHTAKIA

*CATMAS—Computational and Theoretical Materials Sciences Group,
Department of Engineering Science and Mechanics, Pennsylvania State
University, University Park, PA 16802-6812, USA*
(fuw101@psu.edu; akhlesh@psu.edu)

We present a theoretical analysis of a remarkable phenomenon evinced by a periodic structurally chiral material—for example, a chiral sculptured thin film (STF) or a chiral liquid crystal—with a central 90°-twist defect illuminated with normally incident, circularly polarized light. Based on the coupled-wave theory (CWT), an approximate but closed-form solution of the relevant boundary-value problem is obtained in terms of a 4×4 CWT transmission matrix. The CWT transmission matrix is decomposed into two terms. The first term favours total transmission in the central part of the Bragg regime of the axially excited, structurally chiral material, while the second term favours total reflection in the whole Bragg regime. When the thickness of the structurally chiral material is relatively small, the second term is dominated by the first, which gives rise to a co-handed transmittance peak in the centre of the Bragg regime. As the thickness increases, the second term becomes significant and interferes with the first term such that the transmission matrix is isomorphic to that of a defect-free structurally chiral material—except in a tiny wavelength-regime wherein the L_∞ -norms of the two terms become identical to engender the total-reflection feature. Hence, the co-handed transmittance peak diminishes (and eventually vanishes) as the thickness increases and is replaced by a cross-handed reflectance peak. The bandwidths of the two peaks depend, in different ways, on the local birefringence of the structurally chiral material.

Keywords: chiral liquid crystal; chiral sculptured thin film;
circular Bragg phenomenon; coupled-wave theory; structural chirality

1. Introduction

Periodic, structurally chiral materials appear in nature (Neville & Caveney 1969; Graham *et al.* 1993; Gould & Lee 1996). These materials can also be synthesized as self-organized cholesteric liquid crystals (CLC) or nanoengineered as chiral sculptured thin films (STF), through a variety of fabrication techniques (de Jeu 1980; Chandrasekhar 1992; Lakhtakia & Weiglhofer 1995; Hodgkinson & Wu 2001; Lakhtakia 2002). The constitutive dyadics of these materials are

helicoidally non-homogeneous in the thickness direction, in effect describing either a left- or a right-handed screw. As a result, such materials exhibit the *circular Bragg phenomenon*: when circularly polarized (CP) light is normally incident on a sufficiently thick slab of such a material, it is substantially reflected—provided the handedness of the incident light is the same as the structural handedness of the structurally chiral material and the free-space wavelength of light lies in a restricted regime called the Bragg regime. In contrast, light of the opposite handedness is scarcely reflected (Venugopal & Lakhtakia 2000a). Thus, in this selective reflection band (de Vries 1951) such materials behave as one-dimensional photonic bandgap structures for light of one circular polarization but not for the other (Kopp *et al.* 1998). This CP-dimorphic optical response property can be exploited for a variety of optical filters and sensors (Jacobs 1992; Lakhtakia *et al.* 2001; Hodgkinson *et al.* 2002).

In general, structural defects in periodic materials produce localized modes of wave resonance within the photonic bandgap or at the band edges. The localized modes can be harnessed for low-threshold lasers, low-loss waveguides and narrow-band filters in photonic systems (Haus & Shank 1974; Yablonovitch 1987) and are used extensively (Marz 1995; Iizuka 2002). Narrowband circular-polarization filters have been fabricated recently by incorporating either a layer defect or a twist defect in the centre of a chiral STF (Hodgkinson *et al.* 2000a,b) following analysis for both chiral STFs (Lakhtakia & McCall 1999; Lakhtakia *et al.* 2000) and CLCs (Yang *et al.* 1999). Also, lasing has been observed in CLCs with central defects (Schmidtke *et al.* 2003).

As stated earlier, in the absence of the central defect, co-handed CP light is substantially reflected in the Bragg regime while cross-handed CP light is not. The central defect creates a narrow transmission peak for co-handed CP light that pierces the Bragg regime. The spectral location of this peak can be manipulated by varying the defect geometry; we assume in the following that the peak lies in the centre of the Bragg regime and that the light is normally incident. Furthermore, we assume that dissipation is negligibly small, so that electromagnetic energy is not absorbed within the device. Computer simulations show that (i) the bandwidth of the narrow transmission peak begins to diminish and (ii) an even narrower peak begins to develop in the reflection spectrum of the cross-handed CP light as the device thickness increases. There is a crossover thickness of the device at which the two peaks are roughly equal in intensity. Further increase in device thickness causes the co-handed transmission peak to vanish, while the cross-handed reflection peak gains its full intensity and then saturates (Kopp & Genack 2002; Wang & Lakhtakia 2003). The bandwidth of the cross-handed reflection peak is a small fraction of that of the co-handed transmission peak displaced by it. By combining the twist and layer defects, Hodgkinson *et al.* (2003) have shown that superior devices to exploit the crossover phenomenon may be realized. As we have pointed out elsewhere (Wang & Lakhtakia 2003), such a crossover phenomenon cannot be exhibited by the commonplace scalar Bragg gratings and is unique to periodic structurally chiral materials.

Kopp & Genack (2002) formulated the existence of a localized CP defect mode to explain the crossover phenomenon when the central defect is a 90°-twist about the helical axis. But the electromagnetic modes in an axially excited CLC or chiral STF are generally not circularly polarized (Nagle & Lakhtakia 1994),

although phase-matching conditions can reduce cross-polarization (Hodgkinson *et al.* 2002). Oldano (2003) pointed out that the defect mode has both localized and non-localized components, although Kopp & Genack (2003) disputed that assertion. Both Oldano and Kopp & Genack agreed that an analytical explanation of the crossover phenomenon is greatly desirable.

Our purpose in this paper is to theoretically analyse the crossover phenomenon. Therefore, we undertake an analysis of the central 90° -twist defect in a chiral STF; our analysis also applying to cholesteric and chiral smectic liquid crystals (Parodi 1975; Chandrasekhar 1992). Our treatment is based on the coupled-wave theory (CWT), which gives rise to approximate but closed-form solutions for axial wave propagation in chiral STFs (McCall & Lakhtakia 2000, 2004). The resulting closed-form expressions of the reflection and transmission coefficients are subjected to mathematical analysis to elucidate the crossover phenomenon.

In this paper the following notation is employed. Column vectors are underlined and enclosed within square brackets, while matrixes are double underlined and similarly bracketed. The superscript T denotes the transpose, while $*$ and \dagger denote the complex conjugate and the Hermitian adjoint, respectively. The L_∞ -norm of a matrix is denoted by $\|\cdot\|_\infty$ (Lütkepohl 1996). The symbols $\underline{\underline{I}}$ and $\underline{\underline{J}}$ represent 2×2 and 4×4 identity matrixes, respectively. The Kronecker delta function is denoted by $\delta_{p,q}$. An $\exp(-i\omega t)$ time-dependence is implicit, with $i = \sqrt{-1}$, ω as the angular frequency of light and t as time.

2. Theoretical analysis

Let the region $0 < z < 2d$ be occupied by a chiral STF with a central twist defect of ϕ , while the half-spaces $z \leq 0$ and $z \geq 2d$ are filled with a homogenous, isotropic, dielectric medium of refractive index n_r ; see figure 1. The axis of non-homogeneity (i.e. helical axis) of the chiral STF is parallel to the z -axis. A plane wave is normally incident on the plane $z=0$ from the lower half-space $z \leq 0$. As a result, the chiral STF is axially excited and reflection and transmission occur in the two half-spaces.

(a) Constitutive relations

The frequency-dependent relative permittivity matrix $\underline{\underline{\epsilon}}(z)$ of the chiral STF is factorable as (Venugopal & Lakhtakia 2000a,b)

$$\underline{\underline{\epsilon}}(z) = \underline{\underline{S}}_z(z) \underline{\underline{S}}_y(\chi_s) \underline{\underline{\epsilon}}_{\text{ref}} \underline{\underline{S}}_y(\chi_s) \text{T} \underline{\underline{S}}_z(z) \text{T}, \quad 0 < z < 2d. \quad (2.1)$$

As most STFs are locally orthorhombic, the reference relative permittivity 3×3 matrix is given by

$$\underline{\underline{\epsilon}}_{\text{ref}} = \begin{bmatrix} \epsilon_b & 0 & 0 \\ 0 & \epsilon_c & 0 \\ 0 & 0 & \epsilon_a \end{bmatrix}, \quad (2.2)$$

where ϵ_a , ϵ_b and ϵ_c are implicit scalar functions of ω . For simplicity, we only consider non-dissipative chiral STFs in this work, for which $\epsilon_{a,b,c}$ are real-valued.

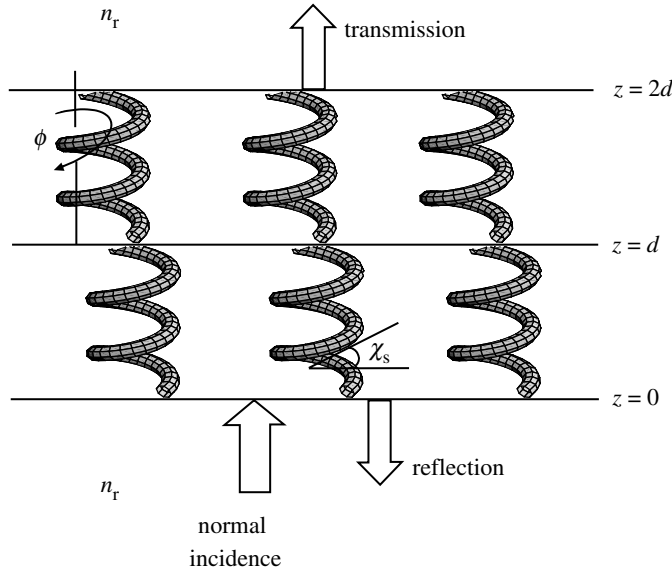


Figure 1. Schematic of the boundary-value problem involving a chiral STF with a central twist defect of $\phi \neq 0^\circ$ about the helical axis introduced between the otherwise identical upper and lower halves. The angle of rise (with respect to the xy plane) of the helical nanowires in a chiral STF is indicated by χ_s .

Dissipation in the CWT formulation of §2*b* can be incorporated, but the additional complications obscure the role of the central twist defect.

The unitary 3×3 matrix

$$[\underline{\underline{S}}_y(\chi_s)] = \begin{bmatrix} \cos \chi_s & 0 & -\sin \chi_s \\ 0 & 1 & 0 \\ \sin \chi_s & 0 & \cos \chi_s \end{bmatrix} \tag{2.3}$$

represents the locally aciculate microstructure, with the angle $\chi_s > 0^\circ$ being the angle of the rise of helical nanowires in the chiral STF. Let us note that $\chi_s = 0^\circ$ and $\epsilon_c = \epsilon_a$ for CLCs. For later convenience, we introduce

$$\tilde{\epsilon}_d = \left(\frac{\cos^2 \chi_s}{\epsilon_b} + \frac{\sin^2 \chi_s}{\epsilon_a} \right)^{-1}, \tag{2.4}$$

which, combined with ϵ_c , suffices for the investigation of axially excited chiral STFs (Venugopal & Lakhtakia 2000*b*).

The rotational non-homogeneity of the chiral STF is captured by the unitary 3×3 matrix

$$[\underline{\underline{S}}_z(z)] = \begin{bmatrix} \cos(pz + \psi) & -h \sin(pz + \psi) & 0 \\ h \sin(pz + \psi) & \cos(pz + \psi) & 0 \\ 0 & 0 & 1 \end{bmatrix}, \tag{2.5}$$

where $p = \pi/\Omega$ and Ω is the structural half-period. The parameter $h=1$ for structural right-handedness, while $h=-1$ for structural left-handedness. The central twist defect is described through the angle

$$\psi = \begin{cases} 0, & 0 < z < d, \\ \phi, & d < z < 2d. \end{cases} \quad (2.6)$$

In the absence of the twist, the two halves of the chiral STF must be identical (Haus & Shank 1974; Lakhtakia & McCall 1999); hence, $N = d/\Omega$ is set as an integer. Furthermore, we set $\phi = 90^\circ$ so as to locate the crossover phenomenon virtually in the middle of the Bragg regime. This agrees with previous numerical studies as well as with a heuristic formula presented by Schmidtke & Stille (2003) for cholesteric liquid crystals.

(b) *Coupled ordinary differential equations*

The frequency-domain Maxwell curl postulates

$$\left. \begin{aligned} \text{curl}[\underline{E}(x, y, z)] &= ik_0[\underline{H}'(x, y, z)], \\ \text{curl}[\underline{H}'(x, y, z)] &= -ik_0[\underline{\underline{\epsilon}}(z)][\underline{E}(x, y, z)] \end{aligned} \right\} 0 < z < 2d, \quad (2.7)$$

are a set of coupled partial differential equations (PDE). Henceforth, the column 3-vector $[\underline{E}(x, y, z)]$ represents the electric field phasor, the column 3-vector $[\underline{H}'(x, y, z)] = \eta_0[\underline{H}(x, y, z)]$, where $[\underline{H}(x, y, z)]$ represents the magnetic field phasor, $\eta_0 = \sqrt{\mu_0/\epsilon_0}$ is the intrinsic impedance of free space (i.e. vacuum), $k_0 = \omega\sqrt{\epsilon_0\mu_0}$ is the free-space wavenumber, and ϵ_0 and μ_0 are the permittivity and the permeability, respectively, of free space.

As we consider the response of the chiral STF to a normally incident plane wave, $[\underline{E}(x, y, z)]$ and $[\underline{H}'(x, y, z)]$ are independent of x and y , that is

$$[\underline{E}(x, y, z)] \equiv [\underline{E}(z)], \quad [\underline{H}'(x, y, z)] \equiv [\underline{H}'(z)]. \quad (2.8)$$

Moreover, by projecting the PDEs (2.7) onto the subspace perpendicular to the z -axis (i.e. the xy plane), we obtain the following set of four ordinary differential equations (ODE) for axial propagation (McCall & Lakhtakia 2004):

$$\left. \begin{aligned} \frac{d}{dz} \left(\begin{bmatrix} 0 & -1 \\ 1 & 0 \end{bmatrix} [\underline{E}_\perp(z)] \right) &= ik_0[\underline{H}'_\perp(z)], \\ \frac{d}{dz} \left(\begin{bmatrix} 0 & -1 \\ 1 & 0 \end{bmatrix} [\underline{H}'_\perp(z)] \right) &= -ik_0[\underline{\underline{\epsilon}}_{\text{perp}}(z)][\underline{E}_\perp(z)], \end{aligned} \right\} 0 < z < 2d. \quad (2.9)$$

Here,

$$[\underline{E}_\perp(z)] = [E_x(z), E_y(z)]^T, \quad [\underline{H}'_\perp(z)] = [H'_x(z), H'_y(z)]^T \quad (2.10)$$

are column 2-vectors,

$$[\underline{\underline{\epsilon}}_{\text{perp}}(z)] = \{[\underline{\underline{\epsilon}}(z)]_\perp^{-1}\}^{-1} \quad (2.11)$$

is a 2×2 matrix and the 2×2 matrix $[\underline{\underline{\epsilon}}(z)]_{\perp}^{-1}$ is obtained by neglecting all components of $[\underline{\underline{\epsilon}}(z)]^{-1}$ on the z -axis.

By simply eliminating $[\underline{H}'_{\perp}(z)]$ in equation (2.9), the matrix ODE

$$\frac{d^2}{dz^2} [\underline{E}_{\perp}(z)] + k_0^2 [\underline{\underline{\epsilon}}_{\text{perp}}(z)] [\underline{E}_{\perp}(z)] = \begin{bmatrix} 0 \\ 0 \end{bmatrix}, \tag{2.12}$$

analogous to the homogeneous Helmholtz equation, is obtained for the axial variation of $[\underline{E}_{\perp}(z)]$. Analytical solution of the second-order ODE (2.12) needs an appropriate expansion of the matrix $[\underline{\underline{\epsilon}}_{\text{perp}}(z)]$. The axial periodicity of chiral STF's suggests that $[\underline{\underline{\epsilon}}_{\text{perp}}(z)]$ can be decomposed into a Fourier series (Yakubovich & Starzhinskii 1975). According to equations (2.1)–(2.6), the Fourier representation of $[\underline{\underline{\epsilon}}_{\text{perp}}(z)]$ in (2.11) is

$$[\underline{\underline{\epsilon}}_{\text{perp}}(z)] = \begin{cases} \tilde{\epsilon}[\underline{I}] + \delta_{\epsilon}[\underline{F}]e^{i2pz} + \delta_{\epsilon}[\underline{F}]^*e^{-i2pz}, & 0 < z < d, \\ \tilde{\epsilon}[\underline{I}] - \delta_{\epsilon}[\underline{F}]e^{i2pz} - \delta_{\epsilon}[\underline{F}]^*e^{-i2pz}, & d < z < 2d, \end{cases} \tag{2.13}$$

where the scalars are

$$\tilde{\epsilon} = (\tilde{\epsilon}_d + \epsilon_c)/2, \quad \delta_{\epsilon} = (\tilde{\epsilon}_d - \epsilon_c)/2, \tag{2.14}$$

and the 2×2 matrix

$$[\underline{F}] = \begin{bmatrix} 1 & -hi \\ -hi & -1 \end{bmatrix}. \tag{2.15}$$

Now, on neglecting the perturbation factor δ_{ϵ} in equation (2.13), the ODE (2.12) yields the solution

$$[\underline{E}_{\perp}(z)] = [\underline{A}^+]e^{ikz} + [\underline{A}^-]e^{-ikz}, \tag{2.16}$$

where $k = k_0\sqrt{\tilde{\epsilon}}$ is the wavenumber in a homogenous, isotropic medium of relative permittivity $\tilde{\epsilon}$ and $[\underline{A}^{\pm}(z)]$ are constant-valued 2-vectors. Therefore, it is natural to render

$$[\underline{E}_{\perp}(z)] = [\underline{A}^+(z)]e^{ikz} + [\underline{A}^-(z)]e^{-ikz}, \tag{2.17}$$

as the solution of ODE (2.12) without ignoring δ_{ϵ} . Thus, equation (2.17) is nothing but a modification of equation (2.16) with variable $[\underline{A}^{\pm}(z)]$ accounting for the periodic nature of $[\underline{\underline{\epsilon}}_{\text{perp}}(z)]$.

Furthermore, in view of the CP-dimorphic optical responses of chiral STF's, it is useful to transform $[\underline{A}^{\pm}(z)]$ into their CP counterparts $[\tilde{\underline{A}}^{\pm}(z)]$ with

$$[\underline{A}^{\pm}(z)] = [\underline{U}][\tilde{\underline{A}}^{\pm}(z)], \tag{2.18}$$

where the transformation matrix is

$$[\underline{U}] = \frac{1}{\sqrt{2}} \begin{bmatrix} 1 & 1 \\ i & -i \end{bmatrix}. \tag{2.19}$$

While the components of the column 2-vectors

$$[\underline{A}^\pm(z)] = \begin{bmatrix} A_x^\pm(z) \\ A_y^\pm(z) \end{bmatrix} \tag{2.20}$$

are understood in the Cartesian coordinate system, the components of the column 2-vectors

$$[\tilde{\underline{A}}^+(z)] = \begin{bmatrix} A_L^+(z) \\ A_R^+(z) \end{bmatrix}, \quad [\tilde{\underline{A}}^-(z)] = \begin{bmatrix} A_R^-(z) \\ A_L^-(z) \end{bmatrix} \tag{2.21}$$

are left CP (LCP) and right CP (RCP), as indicated by the subscripts _L and _R.

By substituting equations (2.13), (2.17) and (2.18) into the ODE (2.12), and enforcing the mutual orthogonalities of LCP and RCP phasors, we derive the following coupled ODEs:

$$\left. \begin{aligned} \frac{1}{k_0^2} \frac{d^2}{dz^2} [\tilde{\underline{A}}^+(z)] + \frac{2ik}{k_0^2} \frac{d}{dz} [\tilde{\underline{A}}^+(z)] &= \mp \delta_\epsilon \{ [\underline{\tilde{F}}^+] [\tilde{\underline{A}}^-(z)] e^{-2i(k-p)z} \\ &\quad + [\underline{\tilde{F}}^-] [\tilde{\underline{A}}^-(z)] e^{-2i(k+p)z} \}, \\ \frac{1}{k_0^2} \frac{d^2}{dz^2} [\tilde{\underline{A}}^-(z)] - \frac{2ik}{k_0^2} \frac{d}{dz} [\tilde{\underline{A}}^-(z)] &= \mp \delta_\epsilon \{ [\underline{\tilde{F}}^+] [\tilde{\underline{A}}^+(z)] e^{2i(k-p)z} \\ &\quad + [\underline{\tilde{F}}^-] [\tilde{\underline{A}}^+(z)] e^{2i(k+p)z} \}. \end{aligned} \right\} \tag{2.22}$$

In these equations, the upper signs (before δ_ϵ) apply for $0 < z < d$ and the lower signs for $d < z < 2d$, while the 2×2 matrixes

$$[\underline{\tilde{F}}^\pm] = \frac{1}{2} \begin{bmatrix} 0 & 1 \mp h \\ 1 \pm h & 0 \end{bmatrix} \tag{2.23}$$

are anti-diagonal. Hence, the ODEs (2.22) decouple $A_L^\pm(z)$ from $A_R^\pm(z)$, but $A_L^-(z)$ is coupled to $A_L^+(z)$ and $A_R^-(z)$ to $A_R^+(z)$.

(c) *Transfer matrixes*

In order to solve the ODEs (2.22), McCall (2001) omitted the second-order derivatives. One reason for that omission is the retrospectively confirmed validity of the inequality $|\frac{d^2}{dz^2} [\tilde{\underline{A}}^\pm(z)]| \ll |k_0 \frac{d}{dz} [\tilde{\underline{A}}^\pm(z)]|$ when $|\delta_\epsilon|/\tilde{\epsilon} \ll 1$. Another reason is to reduce the number of boundary conditions needed for a unique solution. However, unlike McCall (2001) and McCall & Lakhtakia (2004), we do not ignore the terms containing $\exp[\pm 2i(k+p)z]$ in the ODEs (2.22), thereby treating both forms of structural chirality in a unified fashion.

After substituting

$$[\tilde{e}^\pm(z)] = [\tilde{A}^\pm(z)]e^{\pm ikz} \tag{2.24}$$

into ODES (2.22) and neglecting the second-order derivatives, we solve the ODEs (2.22) to obtain the algebraic expressions

$$\begin{bmatrix} [\tilde{e}^+(z)] \\ [\tilde{e}^-(z)] \end{bmatrix} = [\underline{W}^+(z - z_0)] \begin{bmatrix} [\tilde{e}^+(z_0)] \\ [\tilde{e}^-(z_0)] \end{bmatrix}, \quad 0^+ \leq z_0, z \leq d^-, \tag{2.25}$$

and

$$\begin{bmatrix} [\tilde{e}^+(z)] \\ [\tilde{e}^-(z)] \end{bmatrix} = [\underline{W}^-(z - z_0)]^T \begin{bmatrix} [\tilde{e}^+(z_0)] \\ [\tilde{e}^-(z_0)] \end{bmatrix}, \quad d^+ \leq z_0, z \leq 2d^-. \tag{2.26}$$

The transfer 4×4 matrixes $[\underline{W}^\pm(z)]$ are defined as

$$[\underline{W}^\pm(z)] = \begin{bmatrix} P_-(z) & 0 & 0 & \pm Q_-(z) \\ 0 & P_+(z) & \pm Q_+(z) & 0 \\ 0 & \pm Q_+^*(z) & P_+^*(z) & 0 \\ \pm Q_-^*(z) & 0 & 0 & P_-^*(z) \end{bmatrix}, \quad 0 \leq z \leq d, \tag{2.27}$$

where

$$P_\pm(z) = e^{\pm ihpz} \left[\cosh(\mathcal{A}_\mp z) + \frac{i(k \mp hp)}{\mathcal{A}_\mp} \sinh(\mathcal{A}_\mp z) \right], \tag{2.28}$$

$$Q_\pm(z) = e^{\pm ihpz} \left[\frac{i\kappa}{\mathcal{A}_\mp} \sinh(\mathcal{A}_\mp z) \right], \tag{2.29}$$

$$\kappa = k_0 \delta_n, \quad \delta_n = \delta_\varepsilon / 2\tilde{n}, \quad \tilde{n} = \sqrt{\varepsilon} \quad \text{and} \quad \mathcal{A}_\pm = \sqrt{\kappa^2 - (k \pm hp)^2}.$$

The structure of $[\underline{W}^\pm(z)]$ confirms the decoupling of LCP and RCP phasors throughout the chiral STF $0 < z < 2d$ within the approximate framework of CWT. Furthermore, we note that neglect of the terms containing $e^{\pm 2i(k+p)z}$ in the ODEs (2.22) would mean that

$$\left. \begin{aligned} P_+(z)\delta_{h,-1} + P_-(z)\delta_{h,1} &\Rightarrow e^{ikz}, \\ Q_+(z)\delta_{h,-1} + Q_-(z)\delta_{h,1} &\Rightarrow 0, \end{aligned} \right\} \tag{2.30}$$

thereby defeating our purpose of explaining the crossover phenomenon described in §1.

(d) *Boundary conditions*

Expressions for $[\underline{E}_\perp(z)]$ and $[\underline{H}'_\perp(z)]$ are to be obtained after combining expressions (2.25) and (2.26) with the boundary conditions on the interfaces

$z=0$, $z=d$ and $z=2d$. The continuity of the tangential components of the electric and magnetic field phasors across these interfaces implies that $[\underline{E}_\perp(z)]$ and $[\underline{H}'_\top(z)] = (ik_0)^{-1} \frac{d}{dz} [\underline{E}_\perp(z)]$ should be continuous, according to the ODEs (2.9).

Consistently with developments in §2c, we define the circular counterparts of $[\underline{E}_\perp(z)]$ and $[\underline{H}'_\top(z)]$ as

$$[\tilde{\underline{E}}_\perp(z)] = [\underline{U}]^\dagger [\underline{E}_\perp(z)] = [\tilde{e}^+(z)] + [\tilde{e}^-(z)] \tag{2.31}$$

and

$$[\tilde{\underline{H}}'_\top(z)] = [\underline{U}]^\dagger [\underline{H}'_\top(z)] = (ik_0)^{-1} \left[\frac{d}{dz} [\tilde{e}^+(z)] + \frac{d}{dz} [\tilde{e}^-(z)] \right], \tag{2.32}$$

respectively. These 2-vectors must be continuous across the interfaces as well, that is,

$$\left. \begin{aligned} [\tilde{\underline{E}}_\perp(z^-)] &= [\tilde{\underline{E}}_\perp(z^+)], \\ [\tilde{\underline{H}}'_\top(z^-)] &= [\tilde{\underline{H}}'_\top(z^+)], \end{aligned} \right\} z \in \{0, d, 2d\}. \tag{2.33}$$

In accordance with expressions (2.25), (2.26), (2.31) and (2.32), we obtain the expressions

$$\begin{bmatrix} [\tilde{\underline{E}}_\perp(z)] \\ [\tilde{\underline{H}}'_\top(z)] \end{bmatrix} = [\underline{Z}^+] \begin{bmatrix} [\tilde{e}^+(z)] \\ [\tilde{e}^-(z)] \end{bmatrix}, \quad z \in \{0^+, d^-\}, \tag{2.34}$$

and

$$\begin{bmatrix} [\tilde{\underline{E}}_\perp(z)] \\ [\tilde{\underline{H}}'_\top(z)] \end{bmatrix} = [\underline{Z}^-] \begin{bmatrix} [\tilde{e}^+(z)] \\ [\tilde{e}^-(z)] \end{bmatrix}, \quad z \in \{d^+, 2d^-\}, \tag{2.35}$$

where the 4×4 matrixes are

$$[\underline{Z}^\pm] = \tilde{n} [\underline{Z}(1/\tilde{n})] \mp \delta_n \begin{bmatrix} 0 & 0 & 0 & 0 \\ 0 & 0 & 0 & 0 \\ 0 & 1 & 0 & -1 \\ 1 & 0 & -1 & 0 \end{bmatrix} \tag{2.36}$$

and

$$[\underline{Z}(\sigma)] = \begin{bmatrix} \sigma & 0 & \sigma & 0 \\ 0 & \sigma & 0 & \sigma \\ 1 & 0 & -1 & 0 \\ 0 & 1 & 0 & -1 \end{bmatrix}. \tag{2.37}$$

Parentetically, we note that the approximation of $[\underline{W}^\pm(z)]$ via expression (2.30) must not be made for the establishment of the boundary conditions (2.34) and

(2.35), which are crucial to provide an analytical explanation of the crossover phenomenon.

We now examine the electromagnetic field in the two half-spaces to obtain the required values of the field phasors at $z=0^-$ and $z=2d^+$. The incident, reflected and transmitted plane waves propagate along the z -axis in the two half-spaces $z<0$ and $z>2d$. Following Venugopal & Lakhtakia (2000*a,b*), and in analogy with expressions (2.24) and (2.31), we represent the electric field phasors in the two half-spaces as

$$\left. \begin{aligned} [\tilde{\underline{E}}_{\perp}(z)] &= [\underline{\mathcal{A}}]e^{ik_{\text{r}}z} + [\underline{\mathcal{R}}]e^{-ik_{\text{r}}z}, & z \leq 0^-, \\ [\tilde{\underline{E}}_{\perp}(z)] &= [\underline{\mathcal{T}}]e^{ik_{\text{r}}(z-2d)}, & z \geq 2d^+, \end{aligned} \right\} \tag{2.38}$$

where $k_{\text{r}} = k_0 n_{\text{r}}$, and the column 2-vectors

$$[\underline{\mathcal{A}}] = \begin{bmatrix} a_{\text{L}} \\ a_{\text{R}} \end{bmatrix}, \quad [\underline{\mathcal{R}}] = \begin{bmatrix} r_{\text{R}} \\ r_{\text{L}} \end{bmatrix}, \quad [\underline{\mathcal{T}}] = \begin{bmatrix} t_{\text{L}} \\ t_{\text{R}} \end{bmatrix} \tag{2.39}$$

comprise amplitudes of the LCP and RCP components of the incident, reflected and transmitted plane waves, respectively. Finally, similarly to equations (2.34) and (2.35), we obtain

$$\begin{bmatrix} [\tilde{\underline{E}}_{\perp}(z)] \\ [\tilde{\underline{H}}'_{\text{T}}(z)] \end{bmatrix} = [\underline{\underline{Z}}^r] \begin{bmatrix} [\underline{\mathcal{A}}] \\ [\underline{\mathcal{R}}] \end{bmatrix}, \quad z = 0^-, \tag{2.40}$$

and

$$\begin{bmatrix} [\tilde{\underline{E}}_{\perp}(z)] \\ [\tilde{\underline{H}}'_{\text{T}}(z)] \end{bmatrix} = [\underline{\underline{Z}}^r] \begin{bmatrix} [\underline{\mathcal{T}}] \\ [\underline{0}] \end{bmatrix}, \quad z = 2d^+, \tag{2.41}$$

where $[\underline{\underline{Z}}^r] = n_{\text{r}}[\underline{\underline{Z}}(1/n_{\text{r}})]$ and $[\underline{0}] = [0, 0]^T$.

(e) Reflection and transmission

By combining equations (2.25), (2.26), (2.34), (2.35), (2.40) and (2.41) with the boundary conditions (2.33), we finally derive an algebraic equation determining the unknown $[\underline{\mathcal{R}}]$ and $[\underline{\mathcal{T}}]$ as

$$\begin{bmatrix} [\underline{\mathcal{T}}] \\ [\underline{0}] \end{bmatrix} = [\underline{\underline{\tau}}] \begin{bmatrix} [\underline{\mathcal{A}}] \\ [\underline{\mathcal{R}}] \end{bmatrix}, \tag{2.42}$$

where the transmission 4×4 matrix

$$[\underline{\underline{\tau}}] = [\underline{\underline{Z}}^r]^{-1}[\underline{\underline{Z}}^-][\hat{\underline{\tau}}][\underline{\underline{Z}}^+]^{-1}[\underline{\underline{Z}}^r] \tag{2.43}$$

employs the matrix

$$[\hat{\underline{\tau}}] = [\underline{\underline{W}}^-(d)][\underline{\underline{Z}}^-]^{-1}[\underline{\underline{Z}}^+][\underline{\underline{W}}^+(d)], \tag{2.44}$$

which does not depend on n_r . Because of structural chirality, $[\underline{W}^-(d)]$ is related to $[\underline{W}^+(d)]$ and $[\underline{Z}^-]$ to $[\underline{Z}^+]$ by a rotational transformation presented in the appendix. Therefore, the CWT transmission matrix $[\hat{\underline{t}}]$ of (2.44), though specified here for the central 90° -twist defect, applies in a general sense for any ϕ .

Although the transmission matrix $[\underline{\tau}]$ seems very complicated, its replacement by $[\hat{\underline{t}}]$ in equation (2.42) is found to generate values of $[\underline{\mathcal{R}}]$ and $[\underline{\mathcal{T}}]$ that exhibit the main spectral features of the circular Bragg phenomenon, as well those due to the presence of the twist defect. In physical terms, the replacement of $[\underline{\tau}]$ by $[\hat{\underline{t}}]$ for solutions of $[\underline{\mathcal{R}}]$ and $[\underline{\mathcal{T}}]$ amounts to ignoring the index-mismatch across the interfaces $z=0$ and $z=2d$. Indeed, when $|\delta_n| \ll \tilde{n}$ and $n_r = \tilde{n}$, the chiral STF can be said to be index-matched to the medium in the two half-spaces and $[\underline{\tau}] \simeq [\hat{\underline{t}}]$ would then be very true.

To analyse the crossover phenomenon, let us set $n_r = \tilde{n}$ and thus minimize the index-mismatch across the interfaces $z=0$ and $z=2d$. Then,

$$\begin{bmatrix} [\underline{\mathcal{T}}] \\ [0] \end{bmatrix} = [\hat{\underline{t}}] \begin{bmatrix} [\underline{\mathcal{A}}] \\ [\underline{\mathcal{R}}] \end{bmatrix} \tag{2.45}$$

yields approximate but closed-form solutions for $[\underline{\mathcal{R}}]$ and $[\underline{\mathcal{T}}]$ as follows.

Let us define the reflection coefficients (r_{LL} , etc.) and the transmission coefficients (t_{LL} , etc.) through the matrix expressions

$$\begin{bmatrix} r_L \\ r_R \end{bmatrix} = \begin{bmatrix} r_{LL} & r_{RL} \\ r_{LR} & r_{RR} \end{bmatrix} \begin{bmatrix} a_L \\ a_R \end{bmatrix}, \quad \begin{bmatrix} t_L \\ t_R \end{bmatrix} = \begin{bmatrix} t_{LL} & t_{RL} \\ t_{LR} & t_{RR} \end{bmatrix} \begin{bmatrix} a_L \\ a_R \end{bmatrix}. \tag{2.46}$$

Cross-polarized quantities have identical subscripts, while co-polarized quantities do not.

Because the crossover phenomenon involves only the co-polarized quantities, closed-form expressions of the cross-polarized reflection and transmission coefficients are not of interest. On neglecting the small value of \hat{Q}_- in $[\underline{W}^+(d)]$ for $|b| \ll 1$, the solution of equation (2.45) results in the co-polarized transmission coefficients

$$\left. \begin{aligned} t_{LL} &= \frac{\hat{P}_-^2 \hat{\Psi}}{\hat{\Psi} + b^2 \hat{Q}_+^2} \delta_{h,1} + \frac{(|\hat{P}_+|^2 - |\hat{Q}_+|^2)^2}{\hat{\Psi} + b^2 \hat{Q}_+^2} \delta_{h,-1}, \\ t_{RR} &= \frac{\hat{P}_-^2 \hat{\Psi}}{\hat{\Psi} + b^2 \hat{Q}_+^2} \delta_{h,-1} + \frac{(|\hat{P}_+|^2 - |\hat{Q}_+|^2)^2}{\hat{\Psi} + b^2 \hat{Q}_+^2} \delta_{h,1}, \end{aligned} \right\} \tag{2.47}$$

and the co-polarized reflection coefficients

$$\left. \begin{aligned} r_{LL} &= -\frac{\hat{P}_-}{\hat{P}_-^*} \left(\frac{b\hat{\Psi} - b^2 \hat{P}_+^* \hat{Q}_+}{\hat{\Psi} + b^2 \hat{Q}_+^2} \right) \delta_{h,1} - \frac{2 \operatorname{Re}[\hat{P}_+ \hat{Q}_+] + b(|\hat{P}_+|^2 + |\hat{Q}_+|^2) + b^2 \hat{P}_+ \hat{Q}_+}{\hat{\Psi} + b^2 \hat{Q}_+^2} \delta_{h,-1}, \\ r_{RR} &= -\frac{\hat{P}_-}{\hat{P}_-^*} \left(\frac{b\hat{\Psi} - b^2 \hat{P}_+^* \hat{Q}_+}{\hat{\Psi} + b^2 \hat{Q}_+^2} \right) \delta_{h,-1} - \frac{2 \operatorname{Re}[\hat{P}_+ \hat{Q}_+] + b(|\hat{P}_+|^2 + |\hat{Q}_+|^2) + b^2 \hat{P}_+ \hat{Q}_+}{\hat{\Psi} + b^2 \hat{Q}_+^2} \delta_{h,1}, \end{aligned} \right\} \tag{2.48}$$

where

$$\left. \begin{aligned} \hat{\Psi} &= (\hat{P}_+^*)^2 + 2b\hat{P}_+^* \hat{Q}_+ + \hat{Q}_+^2, \\ \hat{P}_\pm &= P_\mp(d)\delta_{h,-1} + P_\pm(d)\delta_{h,1}, \\ \hat{Q}_\pm &= Q_\mp(d)\delta_{h,-1} + Q_\pm(d)\delta_{h,1}. \end{aligned} \right\} \quad (2.49)$$

Reflectances and transmittances are defined as $R_{LL}=|r_{LL}|^2$ and $T_{LL}=|t_{LL}|^2$ and so on. Co-polarized quantities subscripted $_{RR}$ (respectively $_{LL}$) are labelled as co-handed and those subscripted $_{LL}$ (respectively $_{RR}$) are labelled as cross-handed, when the chiral STF is structurally right- (respectively left-)handed. All the results presented in §3 for the chiral STF with a central 90°-twist defect are obtained from the coefficients (2.47) and (2.48), unless otherwise noted.

3. Results and analysis

(a) Chiral STF without defect

For phenomenological completeness, let us begin with the optical response of a chiral STF without the central twist defect. The transmission matrix is then given as

$$[\hat{\underline{\tau}}] = [\underline{W}^+(d)]^2 = [\underline{W}^+(2d)], \quad (3.1)$$

in lieu of equation (2.44).

Figure 2 shows the reflectances and transmittances for $\lambda_0 \in [640, 740]$ nm, when $\epsilon_c = 1.7029^2$, $\tilde{\epsilon}_d = 1.7427^2$, $n_r = \tilde{n} = 1.7230$, $h = 1$, $\Omega = 200$ nm and $N = 50$. The circular Bragg phenomenon is indicated by a peak in R_{RR} and a trough in T_{RR} because the chosen chiral STF is structurally right-handed. The incident LCP plane wave is mostly transmitted. According to CWT, the Bragg regime is centred at the wavelength (McCall & Lakhtakia 2000)

$$\lambda_{0\text{CWT}}^{\text{Br}} = 2\tilde{n}\Omega. \quad (3.2)$$

From numerous calculations, it was ascertained that substantial development of circular Bragg phenomenon requires (Wang 2005)

$$2|b|d \geq \Omega, \quad (3.3)$$

where $b = \delta_n/\tilde{n}$ is the relative local birefringence.

The emergence of the circular Bragg phenomenon can be analytically explained by the characteristics of $[\underline{W}^+(z)]$. This 4×4 matrix can be decomposed into the 2×2 submatrixes

$$[\underline{W}_L^+(z)] = \begin{bmatrix} P_-(z) & Q_-(z) \\ Q_-^*(z) & P_-^*(z) \end{bmatrix}, \quad [\underline{W}_R^+(z)] = \begin{bmatrix} P_+(z) & Q_+(z) \\ Q_+^*(z) & P_+^*(z) \end{bmatrix}, \quad (3.4)$$

which control the responses of the chiral STF to incident LCP and RCP plane waves, respectively. For $|b| \ll 1$, $|Q_\mp(z)|$ is much smaller than $|P_\mp(z)|$ (≈ 1) for $h = \pm 1$. Therefore, $[\underline{W}_R^+(z)]\delta_{h,-1} + [\underline{W}_L^+(z)]\delta_{h,1}$ is approximately equal to the identity matrix for $\lambda_0 \sim \lambda_{0\text{CWT}}^{\text{Br}}$, which leads to total transmission of the

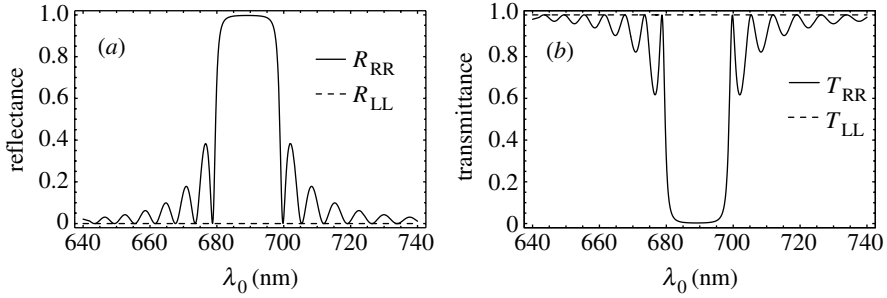


Figure 2. Planewave spectra of (a) reflectances R_{RR} and R_{LL} and (b) transmittances T_{RR} and T_{LL} , calculated for a structurally right-handed chiral STF without the central twist defect for normal incidence. The following parameters were used for CWT calculations: $\epsilon_c = 1.7029^2$, $\tilde{\epsilon}_d = 1.7427^2$, $n_t = \tilde{n} = 1.7230$, $h = 1$, $\mathcal{Q} = 200$ nm, and $N = 50$. Interchange the subscripts L and R for $h = -1$.

incident cross-handed CP light in the Bragg regime. In other words, a chiral STF acts as a homogenous, isotropic, dielectric medium for a normally incident, cross-handed, CP plane wave. However, $[\underline{W}_L^+(z)]\delta_{h,-1} + [\underline{W}_R^+(z)]\delta_{h,1}$ resembles the scattering matrix of a scalar Bragg grating (Haus & Shank 1974). Accordingly, for wavelengths within the Bragg regime, the response to a co-handed CP plane wave is the same as of a scalar Bragg grating (McCall 2001).

(b) Chiral STF with a central 90°-twist defect

Figures 3 and 4 show the spectrums of the co-polarized reflectances and transmittances obtained from the CWT expressions (2.47) and (2.48) when $N=50$ and $N=300$, respectively. As expected, the CWT captures the already-known phenomena that

- a co-handed transmittance peak occurs in the centre of the Bragg regime (figure 3b) for relatively small N which disappears for large N and
- a cross-handed reflectance peak occurs in the centre of the Bragg regime (figure 4a) for large N .

Whereas the former had been predicted by both full electromagnetic analysis (FEMA; Lakhtakia & McCall 1999) as well as CWT (McCall 2003) and verified experimentally (Hodgkinson *et al.* 2000b), the latter had not been predicted by CWT until now. Typically, the bandwidth of the cross-handed reflectance peak is extraordinarily small, and is independent of N beyond its crossover value.

In order to analyse the consequences of introducing the central 90°-twist defect, we take recourse to the matrix $[\hat{\underline{\tau}}]$. This matrix can be decomposed as

$$[\hat{\underline{\tau}}] = [\underline{W}^-(d)][\underline{W}^+(d)] + [\underline{W}^-(d)][\underline{\Theta}(b)][\underline{W}^+(d)], \tag{3.5}$$

where all non-zero entries of the 4×4 matrix

$$[\underline{\Theta}(b)] = [\underline{Z}^-]^{-1}[\underline{Z}^+] - [\underline{\mathfrak{S}}] \tag{3.6}$$

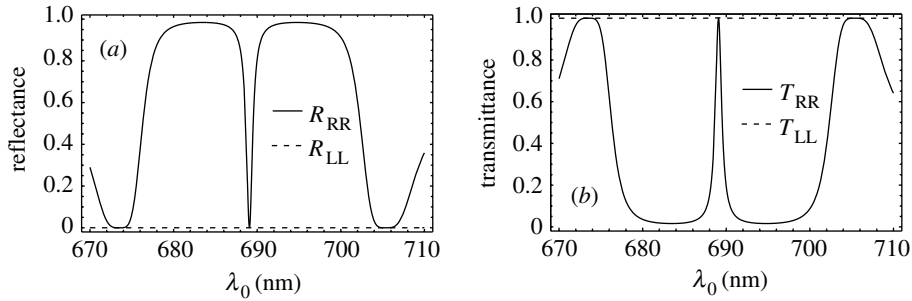


Figure 3. Planewave spectrums of (a) reflectances R_{RR} and R_{LL} and (b) transmittances T_{RR} and T_{LL} , calculated using equations (2.47) and (2.48) for a structurally right-handed chiral STF with a central 90° -twist defect. While the thickness of each chiral STF section is 50Ω (i.e. $N=50$), other parameters are the same as for figure 2. The co-handed transmittance peak in the spectrum of T_{RR} must be noted.

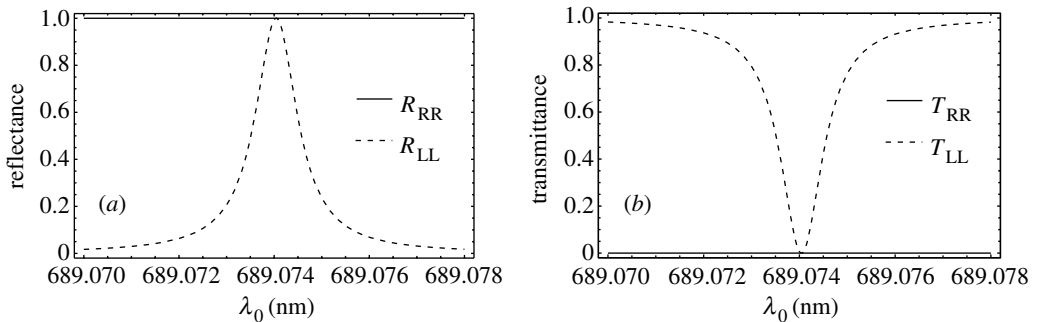


Figure 4. Same as figure 3, but for $N=300$. The cross-handed reflectance peak in the spectrum of R_{LL} must be noted.

are of $\mathcal{O}(b)$. This decomposition is not arbitrary but has physical meaning. The first term on the right side of equation (3.5), all by itself, would give rise to total transmission in the central part of the Bragg regime. In contrast, were $[\hat{r}] = [\underline{W}^-(d)][\underline{\mathcal{Q}}(b)][\underline{W}^+(d)]$, total reflection would occur in the entire Bragg regime, for all $N \geq \frac{1}{2}|b|$. Thus, the second term on the right side of equation (3.5) describes a CP mirror.

As $|b| \ll 1$, the second term on the right side of equation (3.5) may be viewed as perturbing the leading term $[\underline{W}^-(d)][\underline{W}^+(d)]$. Even so, the former is essential to the elucidation of the crossover phenomenon. For convenience, let us define the weight of the second term in relation to the first term as follows:

$$\alpha_\infty = \frac{\|[\underline{W}^-(d)][\underline{\mathcal{Q}}(b)][\underline{W}^+(d)]\|_\infty}{\|[\underline{W}^-(d)][\underline{W}^+(d)]\|_\infty} = \frac{|b|}{1-b^2} \frac{|\hat{P}_+|^2 + |\hat{Q}_+|^2}{|\hat{P}_+^2 + (\hat{Q}_+^*)^2|}. \tag{3.7}$$

According to equation (2.49),

$$\alpha_\infty \approx \begin{cases} |b|, & \text{for } |b \sinh(\pi b N)| \ll 1, \\ |b/\beta|, & \text{for } |b \sinh(\pi b N)| \gg 1, \end{cases} \tag{3.8}$$

where $\beta = (k-p)/\kappa$. Clearly, α_∞ is independent of N in either of the N -ranges specified in equation (3.8). Therefore, both terms on the right side of equation (3.5) are similar to each other in the sense of L_∞ norms in those two N -ranges. Furthermore, a wavelength-regime can be mapped to a β -regime uniquely. $\lambda_0 = \lambda_{0\text{CWT}}^{\text{Br}}$ when $\beta=0$; therefore, the neighbourhood of $\lambda_{0\text{CWT}}^{\text{Br}}$ can be equivalently specified through the β -neighbourhood of 0.

When N is relatively small (but larger than $\frac{1}{2}|b|$), $\|[\underline{W}^\pm(d)]\|_\infty = \mathcal{O}(1)$ and $\alpha_\infty \approx |b| \ll 1$; thus, the second term on the right side of (3.5) can be ignored in favour of the first term, so that $[\hat{\underline{T}}] \approx [\underline{W}^-(d)][\underline{W}^+(d)]$. According to equations (2.28) and (2.29), $[\underline{W}^-(d)][\underline{W}^+(d)]$ becomes almost equal to $[\underline{\mathfrak{T}}]$ for $\lambda_0 \sim \lambda_{0\text{CWT}}^{\text{Br}}$, which gives rise to almost total transmission in the centre of the Bragg regime, as confirmed by figure 3b for $N=50$. In other words, the chiral STF with the central 90° -twist defect becomes optically transparent in a small neighbourhood of $\lambda_{0\text{CWT}}^{\text{Br}}$ for both LCP and RCP plane waves. Another interpretation is that the phase difference between the field phasors at $z=0^+$ and $z=d^-$ is exactly the opposite of the phase difference between the field phasors at $z=d^+$ and $z=2d^-$.

When N is significantly large, the foregoing picture changes completely. $[\hat{\underline{T}}]$ can no longer be considered approximately equal to $[\underline{W}^-(d)][\pm \underline{W}^+(d)]$ because $\alpha_\infty \approx |b/\beta| \rightarrow +\infty$ as $\lambda_0 \rightarrow \lambda_{0\text{CWT}}^{\text{Br}}$. The first term on the right side of equation (3.5) is still almost equal to $[\underline{\mathfrak{T}}]$ at $\lambda_0 = \lambda_{0\text{CWT}}^{\text{Br}}$ —and therefore indicates total transmission in the central part of the Bragg regime all by itself—although the bandwidth of that feature falls exponentially as N increases. But, the second term interferes with the first term in the neighbourhood of $\lambda_{0\text{CWT}}^{\text{Br}}$ so that $[\hat{\underline{T}}]$ is isomorphic to the transmission matrix of a defect-free chiral STF—except in a tiny neighbourhood of $\beta = b$ wherein $\alpha_\infty \approx 1$. It must be the L_∞ -norm-equivalence of the two terms that engenders the total-reflection feature in the tiny neighbourhood of $\beta = b$, as confirmed by figure 4a for $N=300$.

An analytical view of the crossover phenomenon is attained by examining the CWT expressions (2.47) and (2.48) when $\beta = b$. Now, $\hat{\Psi} \equiv 1$ for any N when $\beta = b$ or λ_0 equals

$$\lambda_{0\text{CWT}}^{\text{p}} = \lambda_{0\text{CWT}}^{\text{Br}}(1 - b^2); \tag{3.9}$$

furthermore, $|\hat{P}_-|^2 = 1 + \mathcal{O}(b^2)$ and

$$\text{Det}\left\{[\underline{W}_L^+(d)]\delta_{h,-1} + [\underline{W}_R^+(d)]\delta_{h,1}\right\} = |\hat{P}_+|^2 - |\hat{Q}_+|^2 \equiv 1 \tag{3.10}$$

for any N . Hence, the values of t_{LL} and t_{RR} in equation (2.47) are generally determined by the denominator $\hat{\Psi} + b^2\hat{Q}_+^2$. Typically, when N is not significantly large so that

$$b^2\hat{Q}_+^2 \approx -\frac{b^2}{1 - b^2} \sinh^2(N\pi b) \tag{3.11}$$

is of $\mathcal{O}(1)$ for $\lambda_0 = \lambda_{0\text{CWT}}^{\text{p}}$, we obtain $\hat{\Psi} + b^2\hat{Q}_+^2 \approx 1$. Hence, $T_{\text{LL}} \rightarrow 1$ and $T_{\text{RR}} \rightarrow 1$ as $\lambda_0 \rightarrow \lambda_{0\text{CWT}}^{\text{p}}$. Correspondingly, the co-handed transmittance peak (as well as total cross-handed transmission) occurs near $\lambda_{0\text{CWT}}^{\text{p}}$ for small values of $N \geq \frac{1}{2}|b|$.

However, as N increases, the value of $|b^2 \hat{Q}_+^2|$ increases rapidly to exceed $\hat{\Psi} = 1$ by a huge margin at $\lambda_0 = \lambda_{0\text{CWT}}^{\text{p}}$. Therefore, $T_{\text{LL}} \rightarrow 0$ and $T_{\text{RR}} \rightarrow 0$ for significantly large N at $\lambda_0 = \lambda_{0\text{CWT}}^{\text{p}}$, leading to the disappearance of total transmission in the centre of the Bragg regime. Instead, equation (2.48) implies that $R_{\text{LL}} \rightarrow 1$ and $R_{\text{RR}} \rightarrow 1$ at $\lambda_0 = \lambda_{0\text{CWT}}^{\text{p}}$ for $N \rightarrow +\infty$, thereby confirming the emergence of the cross-handed reflection peak (as well as total co-handed reflection) for large values of $N \geq \frac{1}{2}|b|$.

Although the foregoing analysis successfully provides a rigorous explanation of the crossover phenomenon for either small or significantly large values of $N \geq \frac{1}{2}|b|$, it is limited by the process of approximation in providing an estimation of N_{co} —the crossover value of N . In fact, when N is close to N_{co} , the denominator $\hat{\Psi} + b^2 \hat{Q}_+^2$ in equations (2.47) and (2.48) becomes almost null-valued for $\lambda_0 = \lambda_{0\text{CWT}}^{\text{p}}$. Therefore, equations (2.47) and (2.48) are not reliable as far as adherence to the principle of conservation of energy is concerned. The reason for this inadequacy is the neglect of the second-order derivatives in the coupled ODEs (2.22).

Parenthetically, although the electromagnetic field in axially excited defect-free chiral STFs can be expressed exactly (Kats, 1971; Lakhtakia & Weighofer 1995) and has been used for chiral STFs with central twist defects (Becchi *et al.* 2004), closed-form expressions of the reflectances and transmittances of chiral STFs with central 90° -twist defects are presented here for the first time. These expressions may be used to calculate the peak wavelength and bandwidth when N is sufficiently different from N_{co} .

(c) Peak locations and bandwidths

Figure 5 provides a comparison of the co-handed transmittance and the cross-handed reflectance obtained using the CWT equation (2.48) with those from the FEMA formulated elsewhere (Hodgkinson *et al.* 2000*b*; Venugopal & Lakhtakia 2000*b*). Clearly, figure 5*a* illustrates that the CWT agrees with the FEMA in modelling the co-handed transmittance peak on a (relatively) coarse wavelength-scale for small values of $N \geq \frac{1}{2}|b|$. However, on a highly refined wavelength-scale, the locations of the cross-handed reflectance peak for large values of N are predicted differently by the CWT and the FEMA; see figure 5*b*.

In fact, according to FEMA, both types of peaks are centred at the wavelength

$$\lambda_{0\text{FEMA}}^{\text{p}} = \lambda_{0\text{CWT}}^{\text{Br}} (1 - 0.5b^2). \quad (3.12)$$

When compared with

$$\lambda_{0\text{FEMA}}^{\text{Br}} = \left(\sqrt{\varepsilon_{\text{c}}} + \sqrt{\varepsilon_{\text{d}}} \right) \Omega, \quad (3.13)$$

which is the FEMA prediction of the centre-wavelength of the Bragg regime (Venugopal & Lakhtakia 2000*b*), we find that $\lambda_{0\text{FEMA}}^{\text{p}} = \lambda_{0\text{FEMA}}^{\text{Br}}$ correct to $\mathcal{O}(b^4)$. The deviation of $\lambda_{0\text{CWT}}^{\text{p}}$ of equation (3.9) from $\lambda_{0\text{FEMA}}^{\text{p}}$ echoes the approximation inherent in the CWT.

Figure 6 provides an assessment of the bandwidths of both types of peaks in relation to the local birefringence. The bandwidth of the co-handed transmittance peak decreases exponentially with N . This is because the factor $b^2 \hat{Q}_+^2$ in equation (2.47) increases exponentially with N , as per equation (3.11).

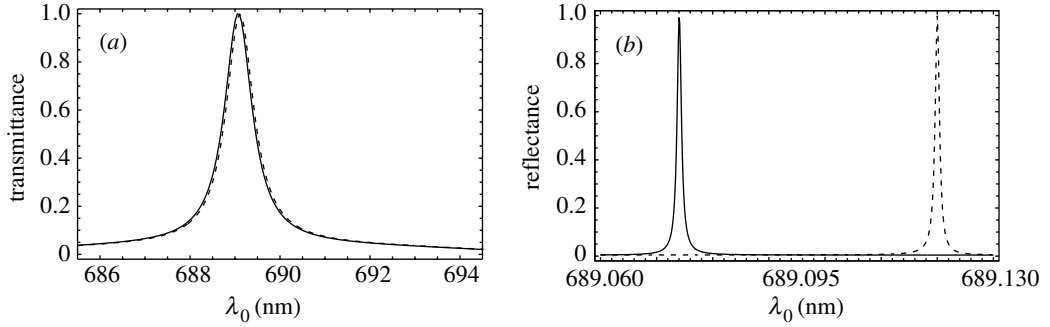


Figure 5. Planewave spectrums of (a) the transmittance T_{RR} for $N=50$ and (b) the reflectance R_{LL} for $N=300$. Other parameters are the same as for figure 3. Data for the solid lines were calculated using the CWT expressions (47) and (48), while the dashed lines are due to FEMA.

The bandwidth of the cross-handed reflectance peak, although saturated for $N > N_{co}$, increases exponentially with $|b|$, as shown in figure 6b. In comparison, figure 6a illustrates that the b -dependence of the bandwidth of the co-handed transmittance peak is linear for $N \geq \frac{1}{2}|b|$.

4. Concluding remarks

In this paper, we presented a theoretical analysis of the optical consequences of introducing a central 90° -twist defect in a chiral sculptured thin film. Our conclusions apply to cholesteric as well as chiral smectic liquid crystals. Based on the coupled-wave theory, we derived an approximate but closed-form solution for axial wave propagation in a chiral STF without the twist defect. This solution greatly facilitated understanding of the consequences of the twist defect's introduction. The CWT transmission matrix of a chiral STF with the twist defect was exploited to obtain approximate but closed-form expressions of the co-polarized reflection and transmission coefficients, with the assumption of index-matching to the ambient medium.

In a nutshell, the CWT transmission matrix of a chiral STF with a central 90° -twist defect can be decomposed as the sum of two terms. The first term—on the right side of equation (3.5)—favors total transmission in the middle of the Bragg regime but the second term favors total reflection in the whole of the Bragg regime. When $N \geq \frac{1}{2}|b|$ is relatively small, the second term is dominated by the first. Therefore, total cross-handed transmittance in the Bragg regime is accompanied by a co-handed transmittance peak in the central part of the Bragg regime. As N increases to some sufficiently large value, the second term becomes significant and interferes with the first term such that the transmission matrix is isomorphic to that of a defect-free chiral STF—except in a tiny neighbourhood of $\lambda_0 = \lambda_{0\text{CWT}}^p$ wherein the two terms become identical to each other in the L_∞ -norm sense to engender the total-reflection feature. Hence, the narrow co-handed transmittance peak diminishes (and eventually vanishes) as N increases and an ultranarrow cross-handed reflectance peak appears. Although our analysis is unable to predict the crossover value of N , it does show that the bandwidths of

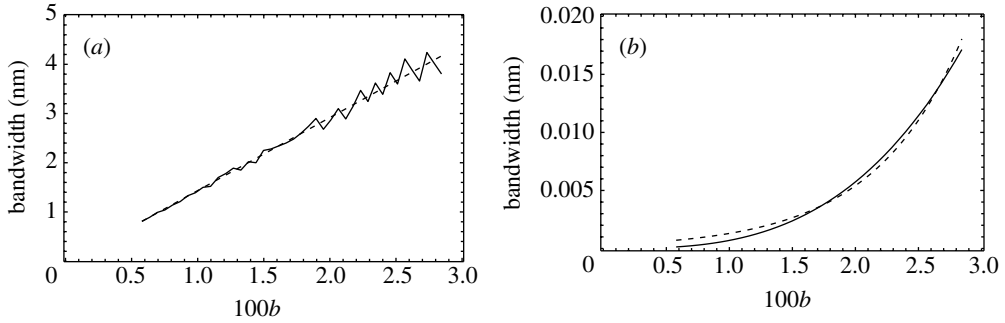


Figure 6. Bandwidths of (a) co-handed transmittance peak for $N=0.5b^{-1}$ and (b) cross-handed reflectance peak for $N=\pi^{-1}b^{-1}\ln(8/b)$ (significantly large), as functions of $b>0$. Data for the solid lines were calculated using equations (2.47) and (2.48), while the dashed lines are fitted to solid lines by (a) a linear function and (b) an exponential function. Other parameters are the same as for figure 3.

the two peaks depend, in different ways, on the local birefringence of the chiral STF. Thus, we have mathematically elucidated the crossover phenomenon.

F.W. thanks the Penn State Weiss Graduate Program for a Dissertation Fellowship.

Appendix A

The matrixes $[\underline{W}^-(d)]$ and $[\underline{W}^+(d)]$ are related in general by

$$[\underline{W}^-(d)] = [\underline{\mathfrak{R}}(\phi)][\underline{W}^+(d)][\underline{\mathfrak{R}}(\phi)]^{-1}, \tag{A 1}$$

where the 4×4 rotational matrix $[\underline{\mathfrak{R}}(\phi)]$ consists of two diagonal blocks as follows:

$$[\underline{\mathfrak{R}}(\phi)] = \begin{bmatrix} [\underline{U}]^\dagger [\underline{R}(\phi)] [\underline{U}] & [\underline{0}] \\ [\underline{0}] & [\underline{U}]^\dagger [\underline{R}(\phi)] [\underline{U}] \end{bmatrix}. \tag{A 2}$$

The 2×2 matrix

$$[\underline{R}(\phi)] = \begin{bmatrix} \cos \phi & -\sin \phi \\ \sin \phi & \cos \phi \end{bmatrix} \tag{A 3}$$

denotes a rotation about the z -axis by an angle ϕ . The matrixes $[\underline{Z}^-]$ and $[\underline{Z}^+]$ are also related via

$$[\underline{\pm Z}^-] = [\underline{\mathfrak{R}}(\phi)][\underline{Z}^+][\underline{\mathfrak{R}}(\phi)]^{-1}. \tag{A 4}$$

When $\phi = m\pi$, where m is an integer, the matrix

$$[\underline{\mathfrak{R}}(\phi)] = [\underline{\mathfrak{I}}]; \tag{A 5}$$

therefore, equations (A 1) and (A 4) simplify to

$$[\underline{W}^-(d)] = [\underline{W}^+(d)], \quad [\underline{Z}^-] = [\underline{Z}^+]. \tag{A 6}$$

As a result, the transmittance matrix is

$$[\hat{\tau}] = [\underline{W}^+(d)]^2 = [\underline{W}^+(2d)], \quad (\text{A } 7)$$

which coincides with equation (3.1) for a defect-free chiral STF (i.e. $\phi=0$).

When $\phi \neq m\pi$, $[\underline{W}^-(d)] \neq [\underline{W}^+(d)]$ in general, which gives rise to the spectral characteristics of $[\hat{\tau}]$ responsible for the crossover phenomenon.

References

- Becchi, M., Ponti, S., Reyes, J. A. & Oldano, C. 2004 Defect mode in helical photonic crystals: an analytic approach. *Phys. Rev. B* **70**, 033103.
- Chandrasekhar, S. 1992 *Liquid crystals*, 2nd edn. Cambridge: Cambridge University Press.
- de Jeu, W. H. 1980 *Physical properties of liquid crystalline materials*. New York: Gordon & Breach.
- de Vries, H. 1951 Rotary power and other optical properties of certain liquid crystals. *Acta crystallogr.* **4**, 219–226.
- Gould, K. S. & Lee, D. W. 1996 Physical and ultrastructural basis of blue leaf iridescence in four Malaysian understory plants. *Am. J. Bot.* **83**, 45–50.
- Graham, R. M., Lee, D. W. & Nortsog, K. 1993 Physical and ultrastructural basis of blue leaf iridescence in two neotropical ferns. *Am. J. Bot.* **80**, 198–203.
- Haus, H. A. & Shank, C. V. 1974 Antisymmetric taper of distributed feedback lasers. *IEEE J. Quantum Electron.* **12**, 532–539.
- Hodgkinson, I. J. & Wu, Q. h. 2001 Inorganic chiral optical materials. *Adv. Mater.* **13**, 889–897.
- Hodgkinson, I. J., Wu, Q. h., Lakhtakia, A. & McCall, M. W. 2000a Spectral-hole filter fabricated using sculptured thin-film technology. *Opt. Commun.* **177**, 79–84.
- Hodgkinson, I. J., Wu, Q. h., Thorn, K. E., Lakhtakia, A. & McCall, M. W. 2000b Spacerless circular-polarization spectral-hole filters using chiral sculptured thin films: theory and experiment. *Opt. Commun.* **184**, 57–66.
- Hodgkinson, I. J., Wu, Q. h., Arnold, M., McCall, M. W. & Lakhtakia, A. 2002 Chiral mirror and optical resonator designs for circularly polarized light: suppression of cross-polarized reflectances and transmittances. *Opt. Commun.* **210**, 201–211.
- Hodgkinson, I. J., Wu, Q. h., De Silva, L., Arnold, M., McCall, M. W. & Lakhtakia, A. 2003 Supermodes of chiral photonic filters with combined twist and layer defects. *Phys. Rev. Lett.* **91**, 223903.
- Iizuka, K. 2002 *Elements of photonics*. New York: Wiley.
- Jacobs, S. D. (ed.) 1992 *Selected papers on liquid crystals for optics*. Bellingham, WA: SPIE Press.
- Kats, E. I. 1971 Optical properties of cholesteric liquid crystals. *Sov. Phys. JETP* **32**, 1004–1007.
- Kopp, V. I. & Genack, A. Z. 2002 Twist defect in chiral photonic structures. *Phys. Rev. Lett.* **89**, 033901.
- Kopp, V. I. & Genack, A. Z. 2003 Reply to comment. *Phys. Rev. Lett.* **91**, 259402.
- Kopp, V. I., Fan, B., Vithana, H. K. M. & Genack, A. Z. 1998 Low-threshold lasing at the edge of a photonic stop band in cholesteric liquid crystals. *Opt. Lett.* **23**, 1707–1709.
- Lakhtakia, A. 2002 Sculptured thin films: accomplishments and emerging uses. *Mater. Sci. Eng. C* **19**, 427–434.
- Lakhtakia, A. & McCall, M. W. 1999 Sculptured thin films as ultranarrow-bandpass circular-polarization filters. *Opt. Commun.* **168**, 457–465.
- Lakhtakia, A. & Weiglhofer, W. S. 1995 On light propagation in helicoidal bianisotropic mediums. *Proc. R. Soc. Lond. A* **448**, 419–437. [Erratum **454**, 3275.]
- Lakhtakia, A., Venugopal, V. C. & McCall, M. W. 2000 Spectral holes in Bragg reflection from chiral sculptured thin films: circular polarization filters. *Opt. Commun.* **177**, 57–68.

- Lakhtakia, A., McCall, M. W., Sherwin, J. A., Wu, Q. h. & Hodgkinson, I. J. 2001 Sculptured-thin-film spectral holes for optical sensing of fluids. *Opt. Commun.* **194**, 33–46.
- Lütkepohl, H. 1996 *Handbook of matrices*. Chichester, UK: Wiley.
- Marz, R. 1995 *Integrated optics: design and modeling*. Boston, MA: Artech House.
- McCall, M. W. 2001 Axial electromagnetic wave propagation in inhomogeneous dielectrics. *Math. Comput. Model.* **34**, 1483–1497.
- McCall, M. W. 2003 Towards optoelectronic applications of chiral sculptured thin films. In *Introduction to complex mediums for optics and electromagnetics* (ed. W. S. Weiglhofer & A. Lakhtakia). Bellingham, WA: SPIE Press.
- McCall, M. W. & Lakhtakia, A. 2000 Development and assessment of coupled wave theory of axial propagation in thin-film helicoidal bianisotropic media. I. Reflectances and transmittances. *J. Mod. Opt.* **47**, 973–991. [Erratum **50**, 2807.]
- McCall, M. W. & Lakhtakia, A. 2004 Explicit expressions for spectral remittances of axially excited chiral sculptured thin films. *J. Mod. Opt.* **51**, 111–127.
- Nagle, S. F. & Lakhtakia, A. 1994 Attenuation and handedness of axial propagation modes in a cholesteric liquid crystal. *Microw. Opt. Tech. Lett.* **7**, 749–752.
- Neville, A. C. & Caveney, S. C. 1969 Scarabaeid beetle exocuticle as an optical analogue of cholesteric liquid crystal. *Biol. Rev.* **44**, 531–562.
- Oldano, C. 2003 Comment on ‘Twist defect in chiral photonic structures’. *Phys. Rev. Lett.* **91**, 259401.
- Parodi, O. 1975 Light propagation along the helical axis in chiral smectics. *C. J. Phys., Paris Colloq.* **36**(C1), 325–326.
- Schmidtke, J. & Stille, W. 2003 Photonic defect modes in cholesteric liquid crystal films. *Eur. Phys. J. E* **12**, 553–564.
- Schmidtke, J., Stille, W. & Finkelmann, H. 2003 Defect mode emission of a dye-doped cholesteric polymer network. *Phys. Rev. Lett.* **90**, 083902.
- Venugopal, V. C. & Lakhtakia, A. 2000 Electromagnetic plane-wave response characteristics of non-axially excited slabs of dielectric thin-film helicoidal bianisotropic mediums. *Proc. R. Soc. Lond. A* **456**, 125–161. (doi:10.1098/rspa.2000.0511.)
- Venugopal, V. C. & Lakhtakia, A. 2000 Sculptured thin films—conception, optical properties, and applications. In *Electromagnetic fields in unconventional materials and structures* (ed. O. N. Singh & A. Lakhtakia). New York: Wiley.
- Wang, F., 2005. Optics of slanted chiral sculptured thin films. PhD dissertation, Pennsylvania State University, University Park.
- Wang, F. & Lakhtakia, A. 2003 Specular and nonspecular, thickness-dependent, spectral holes in a slanted chiral sculptured thin film with a central twist defect. *Opt. Commun.* **215**, 79–92.
- Yablonovitch, E. 1987 Inhibited spontaneous emission in solid-state physics and electronics. *Phys. Rev. Lett.* **58**, 2059–2062.
- Yakubovich, V. A. & Starzhinskii, V. M. 1975 *Linear differential equations with periodic coefficients*. Chichester, UK: Wiley.
- Yang, Y. C., Kee, C. S., Kim, J. E., Park, H. Y., Lee, J. C. & Jeon, Y. J. 1999 Photonic defect modes of cholesteric liquid crystals. *Phys. Rev. B* **60**, 6852–6854.